JOURNAL OF MATERIALS SCIENCE 8 (1973) 23–36

Deformation mechanisms in oriented high-density polyethylene

R. J. YOUNG, P. B. BOWDEN
Department of Metallurgy and Materials Science, Pembroke Street, Cambridge, UK

J. M. RITCHIE, J. G. RIDER
Physics Department, University of Surrey, Guildford UK

The deformation of samples of oriented high-density polyethylene has been analysed in terms of three principal deformation mechanisms, *fibrillar slip, lamella slip* and *chain slip.* From a study of small- and wide-angle X-ray diffraction patterns it is possible to deduce which mechanism or mechanisms are operating in particular cases. Material prepared in three different ways has been examined and it appears that in all three cases the primary mechanism for plastic deformation is [001] chain slip.

In oriented and annealed material with a well-defined lamella crystal structure it has been possible to show that the recoverable elastic deformation is primarily due to reversible lamella slip. In this material plastic deformation by chain slip starts at a well-defined critical resolved shear stress of about 15 MNm^{-2}.

Deformation of oriented unannealed material, in which the crystal structure is not so well-defined, appears to be more complicated. In material prepared by cold drawing some of the plastic strain may be accounted for by permanent lamella slip. Fibrillar slip does not appear to be a major deformation mechanism in any of the three materials.

1. Introduction

Crystalline polyethylene that has been oriented by drawing or by other means has a structure which in outline appears to be relatively simple although the details are by no means settled [1]. The structure is fibrous. Most of the molecular chains are aligned in the orientation direction and are incorporated in planar chain-folded crystals. The crystals are separated by amorphous rubbery polymer and are to some extent tied together by intercrystalline link molecules.

We have studied the deformation of samples of oriented polyethylene prepared in various ways and have attempted to explain our results in terms of three principal deformation mechanisms. For a more complete discussion of deformation mechanisms see [2].

2. Deformation mechanisms

Oriented specimens were compressed between parallel dies with the orientation direction at an angle to the compression direction as illustrated schematically in Fig. 1. This type of loading favours simple shear deformations parallel and perpendicular to the chain axis. It was observed experimentally in all cases that the deformation approximated closely to plane strain; there were no strains perpendicular to the plane of Fig. 1 except where noted as bulging.

2.1. Fibrillar slip

The model we have used for the structure of oriented polyethylene is shown schematically in Fig. 1a. It is suggested that the stacked crystals are organized in fibrils that are capable of shearing relative to each other as shown schematically in Fig. 1b. On compression such a shear will cause the chain axis, c, and the lamella normal, n, to rotate together away from the compression direction.

2.2. Lamella slip

A second method of deformation is by shear of the lamella crystals over each other. In this case both c and n will rotate together towards the compression direction as illustrated in Fig. 1c.

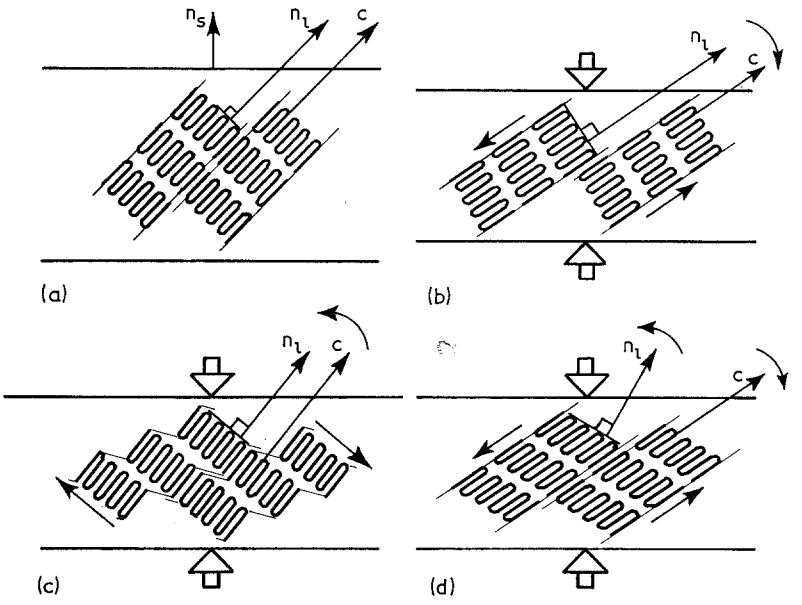

Figure 1 Schematic diagram of the structure of oriented polyethylene. It is assumed that the molecules are folded to form lamella crystals which are incorporated into fibrils. c defines the chain direction, n_c is the surface normal of the lamella crystals and n_s is the surface normal of the specimen which is parallel to the compression direction. (a) The structure before deformation; (b) after deformation by fibrillar slip; (c) after deformation by lamella slip and (d) after deformation by chain slip.

2.3. Chain slip

If the crystals themselves deform by crystallographic slip parallel to the chain direction then the consequences will be as illustrated in Fig. 1d. The chain axis, c, will rotate away from the compression direction while the lamella normal, n, remains approximately in its original position. This is the only type of deformation for which the angle between c and n changes as the deformation proceeds.

3. Analysis of the deformation

3.1. Fibrillar slip

The fibrillar slip process is illustrated in Fig. 2. In the figure one half of the sample has been deformed to a shear strain of γ_F; h is the thickness of the sample, θ is the angle between the chain direction, c, and the surface normal, n_S (the compression direction), and ϕ is the angle between the lamella normal n_l and the surface normal. The suffixes 0 and 1 denote values before and after the shear has occurred. It follows from the geometry of the figure that

$$\gamma_F = \tan\theta_1 - \tan\theta_0 \qquad (1)$$

$$\frac{h_1}{h_0} = \frac{\cos\theta_1}{\cos\theta_0} \qquad (2)$$

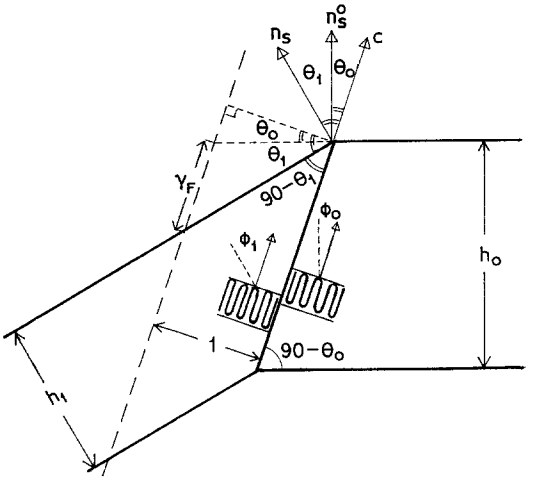

Figure 2 The geometry of deformation by fibrillar slip.

and, since the angle between the lamella normal and the chain direction remains unchanged during the deformation

$$(\theta - \phi) \text{ is constant} . \qquad (3)$$

By differentiation of Equations 1, 2 and 3 the following expressions can be obtained:

$$\delta\theta_F = \delta\gamma_F \cos^2\theta \qquad (4)$$

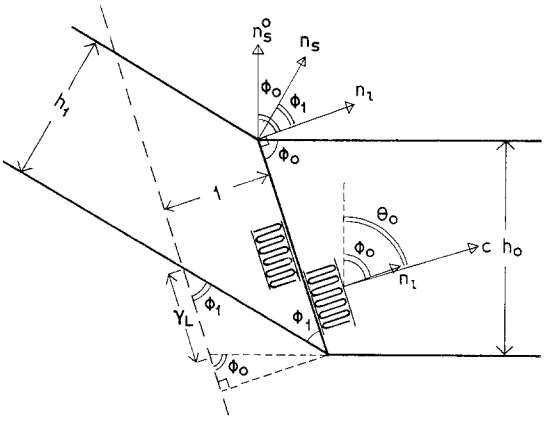

Figure 3 The geometry of deformation by lamella slip.

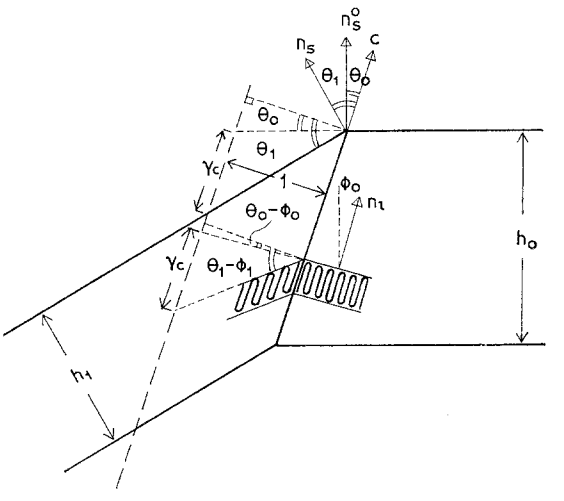

Figure 4 The geometry of deformation by chain slip.

$$-\frac{\delta h_F}{h} = \delta\gamma_F \sin\theta\cos\theta \quad (5)$$

$$\delta\phi_F = \delta\theta_F = \delta\gamma_F \cos^2\theta\ . \quad (6)$$

3.2. Lamella slip

This process is illustrated in Fig. 3, which shows a sample one half of which has been deformed in simple shear on planes parallel to the lamellae to a strain of γ_L. Using the same convention as before it follows from the geometry that:

$$\gamma_L = \cos\phi_1 - \cot\phi_0 \quad (7)$$

$$\frac{h_1}{h_0} = \frac{\sin\phi_1}{\sin\phi_0} \quad (8)$$

$$(\theta - \phi) \text{ is constant}\ . \quad (9)$$

By differentiation of Equations 7, 8 and 9

$$\delta\theta_L = \delta\phi_L \quad (10)$$

$$-\frac{\delta h_L}{h} = \delta\gamma_L \sin\phi\cos\phi \quad (11)$$

$$\delta\phi_L = -\delta\gamma_L \sin^2\phi\ . \quad (12)$$

3.3. Chain slip

The situation when chain slip occurs is a little more complicated since the orientation of the lamellae normal changes relative to the chain axis during the deformation. The geometry of the process is illustrated in Fig. 4 for a shear of γ_C parallel to the chain direction. It follows from the figure that

$$\gamma_C = \tan\theta_1 - \tan\theta_0\ , \quad (13)$$

$$\frac{h_1}{h_0} = \frac{\cos\theta_1}{\cos\theta_0} \quad (14)$$

and also

$$\gamma_C = \tan(\theta_1 - \phi_1) - \tan(\theta_0 - \phi_0)\ . \quad (15)$$

By differentiation it can be shown that

$$\delta\theta_C = \delta\gamma_C \cos^2\theta\ , \quad (16)$$

$$-\frac{\delta h_C}{h} = \delta\gamma_C \sin\theta\cos\theta\ , \quad (17)$$

and

$$\delta\phi_C = \delta\gamma_C(\cos^2\theta - \cos^2(\theta - \phi))\ . \quad (18)$$

3.4. A general deformation

There are three quantities that it is possible to measure experimentally on a deforming sample. The strain applied, $\delta h/h$, can be measured directly. The instantaneous value of θ, the orientation of the chain axes, can be obtained from a wide-angle X-ray diffraction pattern; and in cases where the lamella crystals are well defined the angle ϕ which specifies their orientation can be obtained from a small-angle X-ray diffraction pattern.

Even if all this information is available it is not possible to analyse a finite general deformation into its three component shears. However, it is possible to analyse a general deformation if it is carried out in small steps and intermediate values of h, θ and ϕ are obtained. For a small increase in applied strain:

$$\delta\theta = \delta\gamma_F \cos^2\theta - \delta\gamma_L \sin^2\phi + \delta\gamma_C \cos^2\theta \quad (19)$$

$$-\frac{\delta h}{h} = \delta\gamma_F \sin\theta\cos\theta + \delta\gamma_L \sin\phi\cos\phi + \delta\gamma_C \sin\theta\cos\theta \quad (20)$$

$$\delta\phi = \delta\gamma_F \cos^2\theta - \delta\gamma_L \sin^2\phi + \delta\gamma_C(\cos^2\theta - \cos^2(\theta - \phi))\ . \quad (21)$$

These three equations can be solved to obtain the three unknowns $\delta\gamma_F$, $\delta\gamma_L$ and $\delta\gamma_C$.

For some of our samples it has not been possible to obtain reliable values for ϕ. For others it has not been possible to do so for each small increase in applied deformation. If the assumption is made that there is no fibrillar shear, then $\delta\gamma_F = 0$ and Equations 19 and 20 can be used to obtain specific solutions for $\delta\gamma_L$ and $\delta\gamma_C$.

$$\delta\gamma_L = \frac{-\left(\delta\theta \sin\theta + \frac{\delta h}{h}\cos\theta\right)}{\sin\phi\cos(\theta - \phi)} \quad (22)$$

$$\delta\gamma_C = \frac{\delta\theta\cos\phi - \frac{\delta h}{h}\sin\phi}{\cos\theta\cos(\theta - \phi)}. \quad (23)$$

The assumption that there has been no fibrillar shear can be checked subsequently by comparing the value of ϕ computed from Equation 21 with that obtained experimentally after a large deformation.

The analysis above in Sections 2 and 3 assumes that only three specific deformation mechanisms occur and that their effects are additive. Provided that the deformation is in plane strain on the molecular scale, and provided the crystalline regions are planar entities as the low-angle X-ray photographs show them to be, at any rate in the annealed material, no additional deformation mechanisms seem at all likely. If shear occurs between or within crystals in directions out of the plane of the diagram in Fig. 1 then the deformation is no longer plane strain and the analysis breaks down. If such deformation mechanisms occur they are likely to result in significant bulging of the sample. Where such bulging occurred it has been noted.

4. Specimen preparation

The material used was a linear polyethylene,

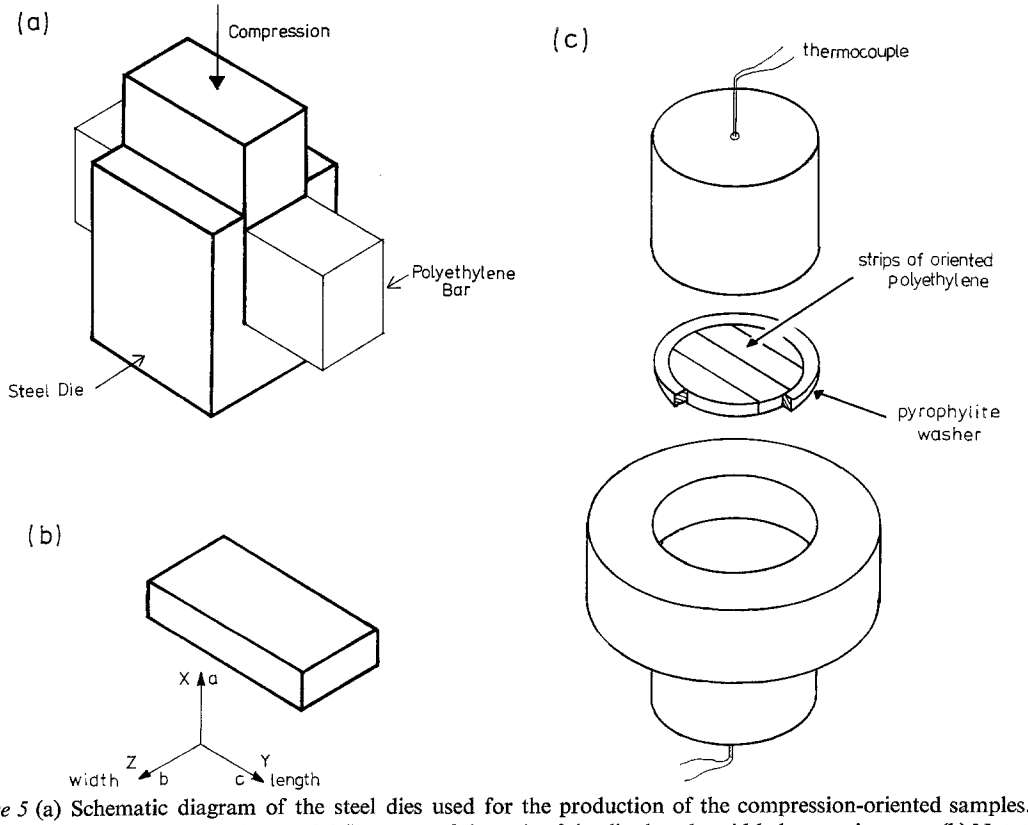

Figure 5 (a) Schematic diagram of the steel dies used for the production of the compression-oriented samples. As the height of the bar is reduced, material flows out of the ends of the dies but the width does not increase. (b) Notation, similar to that in [2], used to define directions in the compression-oriented and annealed samples. The diagram is in the same orientation as (*a*) and (*c*). The crystal axes *a* and *b* are parallel to *x* and *z* respectively only after annealing under pressure. (c) A diagram of the steel dies used for annealing the oriented material under pressure.

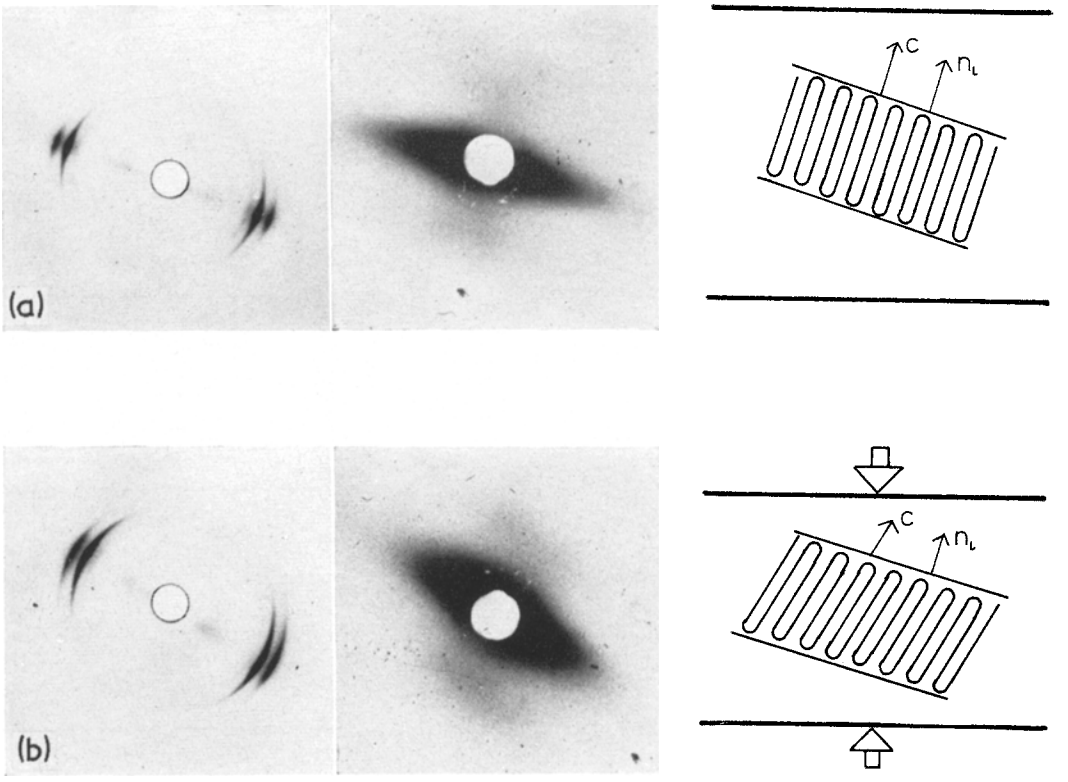

Figure 6 Wide- and low-angle X-ray diffraction patterns of the draw-oriented samples taken with the beam perpendicular to the orientation direction. The schematic diagrams are of the molecular structure within the crystal lamellae as deduced from the diffraction patterns. (a) Before deformation $\theta_0 = 20°$; (b) after compression to a permanent plastic strain of 16.3%.

Rigidex 9, supplied by British Petrochemicals Ltd in the form of granules. These were injection moulded into tensile specimens with a rectangular cross-section 6 × 13 mm. The density as moulded was 0.95 g ml^{-1}.

4.1. Draw-oriented sample

Tensile specimens were drawn at 22 ± 2°C at an initial strain-rate of 0.023 min^{-1} to their natural draw ratio which at this strain-rate is about 5. The material had a white silky appearance and had a density of 0.91 g ml^{-1}. From wide-angle X-ray photographs we inferred that the *c*-axes were oriented along the draw direction and the *a*- and *b*-axes were randomly oriented around the draw direction. The low-angle X-ray diffraction photographs (Fig. 6) taken with the X-ray beam perpendicular to the chain direction was not very well defined and there was a void streak perpendicular to the chain direction.

4.2. Compression-oriented sample

The central regions of the injection moulded bars were compressed in the die shown schematically in Fig. 5a at 22 ± 2°C at an initial strain-rate of 0.33 min^{-1}. The height was reduced by a factor of about 7 from 13 to 1.8 mm. As the height was reduced the length increased but within the dies the width remained constant at 6 mm. After compression the material was transparent with a density of 0.952 g ml^{-1} and wide-angle X-ray diffraction photographs of the material were similar to those obtained for "drawn and rolled" material described by Hay and Keller [3]. For both materials the photographs are consistent with a texture in which the *c*-axis is oriented along the length of the specimen (*y*), the *a*-axis is along *x* and the *b*-axis is along *z*, and the structure is heavily twinned on {1 1 0} planes. There was also a strong reflection corresponding to the monoclinic α-spacing of 4.5Å. The small-angle X-ray

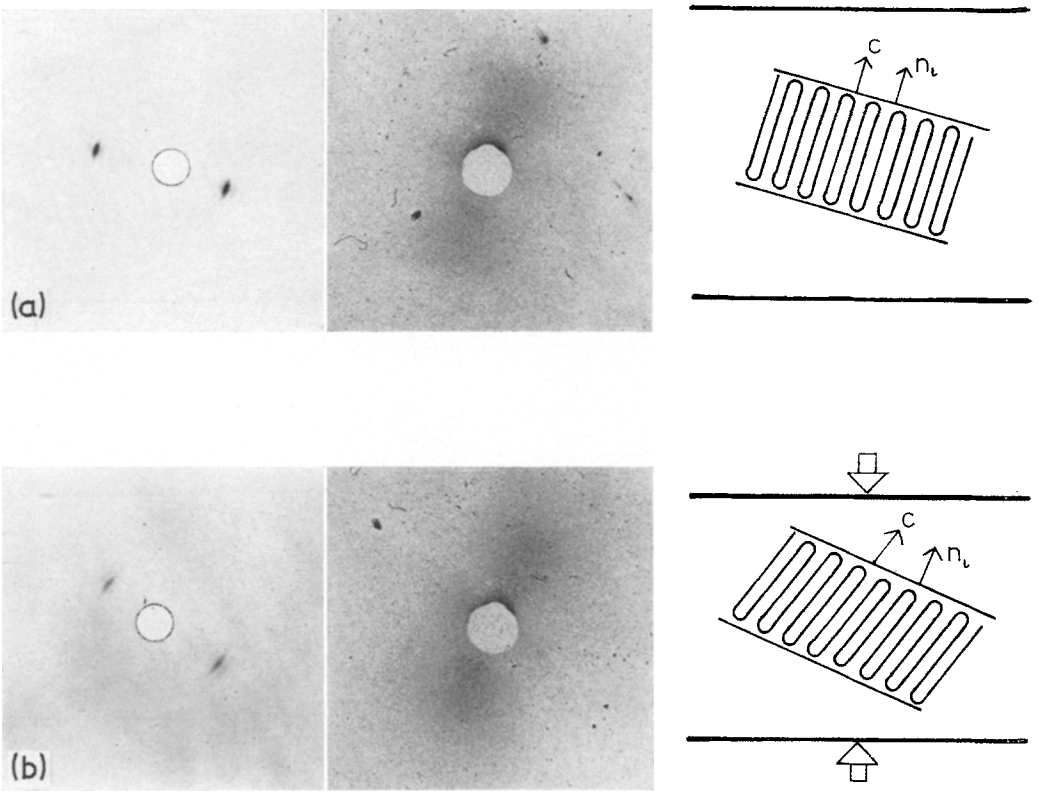

Figure 7 Wide- and low-angle X-ray diffraction patterns for the compression-oriented material. The beam is along the x-direction. (a) Before deformation $\theta_0 = 18.5°$; (b) after compression to a permanent plastic strain of 15.1%.

pattern (Fig. 7) taken with the beam along the x direction showed a distribution of lamella spacings from 100 to 200Å.

4.3. Annealed sample

Compression-oriented samples were annealed under hydrostatic pressure. A number of them were laid side by side and cut into a circular disc shape. The disc was laid inside a pyrophylite washer between steel dies 25 mm in diameter as shown in Fig. 5c. The dies were then sandwiched between a pair of electrically heated and water cooled platens and the whole sandwich was put in a press. The load was increased until the calculated pressure in the sample reached 4 kbar and the platens were then used to heat the system to the annealing temperature. After annealing at 200°C for 15 min the sample was quenched by water cooling the platens to room temperature before releasing the pressure. The material was still transparent and its density had increased to 0.966 g ml^{-1}. The spread of the a-, b- and c-axes orientations had decreased and the material now had a single-crystal texture [3] with the crystal axes related to the sample axes as shown in Fig. 5b. The small-angle X-ray diffraction pattern shown in Fig. 8a taken with the beam along the X direction is very well defined, indicating that the structure is made up of lamella crystals with a repeat distance of 290 $\pm$ 10Å with the projections of their surface normals in the yz plane in Fig. 5b lying approximately parallel to the chain direction.

5. Stress-strain results

Samples were cut from the oriented material in the yz plane at various angles to the c-direction. They were compressed between lubricated dies as shown in Fig. 9 and as described previously by two of us [4]. Deformation was carried out at 25 $\pm$ 0.5°C on an "E-type" Tensometer at a constant cross-head speed, which in all cases corresponded to an initial strain-rate of 0.16 min^{-1}.

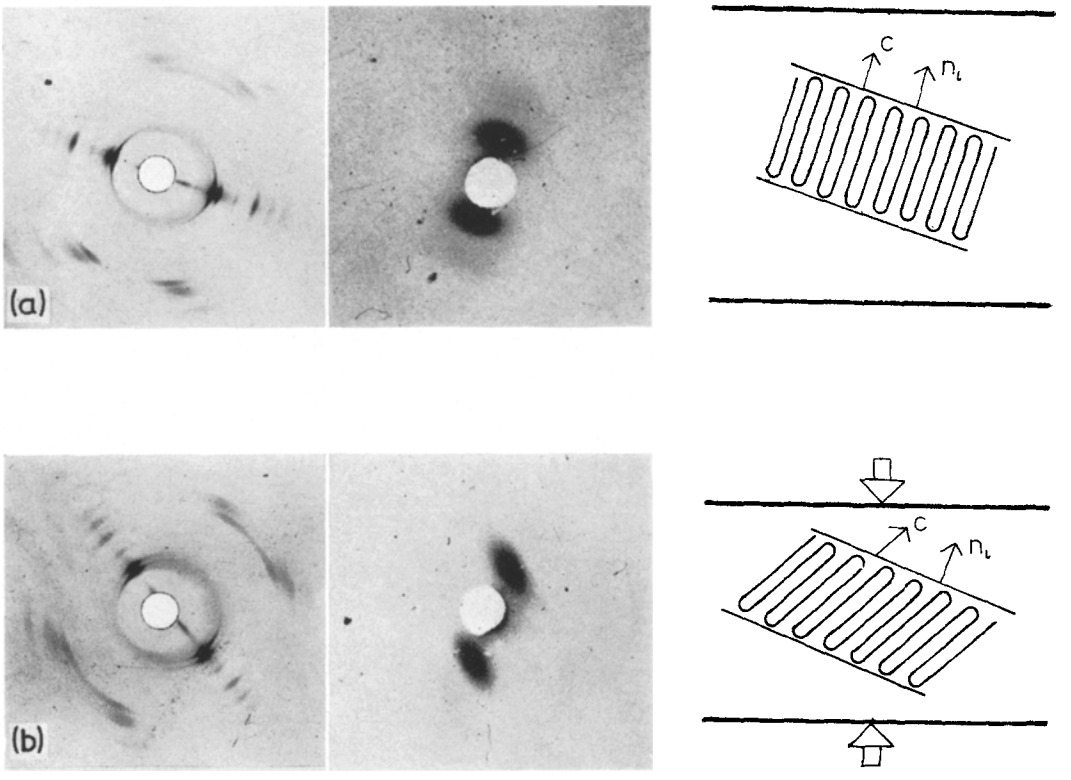

Figure 8 Wide- and low-angle X-ray diffraction patterns of the annealed material with the beam along the *x*-direction. (a) Before deformation $\theta_0 = 17.5°$; (b) after compression to a permanent plastic strain of 27.6%.

Specimens having θ_0 values of approximately 20°, 40° and 60° were prepared for each of the three types of material investigated. Three stress-strain curves for each material were then obtained. The angles of the chain axes to the compression direction were measured by wide-angle X-ray diffraction. The stress was calculated by dividing the load by the area ($w_0 b$). In all cases up to compressive strains of 40% the bulging was less than 6% which meant that the specimens deformed approximately in plane strain. Since the area under the dies did not change by very much this stress approximates to a true stress.

To produce a plot of stress versus θ, the instantaneous value of θ was calculated from the change in height using Equation 2 which assumes that deformation occurs by simple shear parallel to the chain direction. The plots of stress against the calculated values of θ for the three different types of material are shown in Fig. 10. If the deformation is by simple shear at a constant critical resolved shear stress of τ the compressive flow stress σ is given by a relation due to Schmid and Boas [5]:

$$\sigma = \tau/(\sin\theta \cos\theta) . \qquad (24)$$

This function is drawn as dashed lines in Fig. 10 fitted for different values of τ for each material.

5.1. Annealed sample

The three curves for this material are plotted as the top set of curves in Fig. 10. It can be seen that they fall on a common envelope and lie close to the theoretical line which in this case is drawn for a critical resolved shear stress of 15.5 MNm^{-2}. This implies that the material is deforming approximately by simple shear parallel to the *c*-axis at a well defined critical shear stress. However the curves do lie a few degrees to the right of the dashed line. The significance of this is discussed in Section 8.3. Samples with densities of above 0.97 g m^{-1} are brittle and do

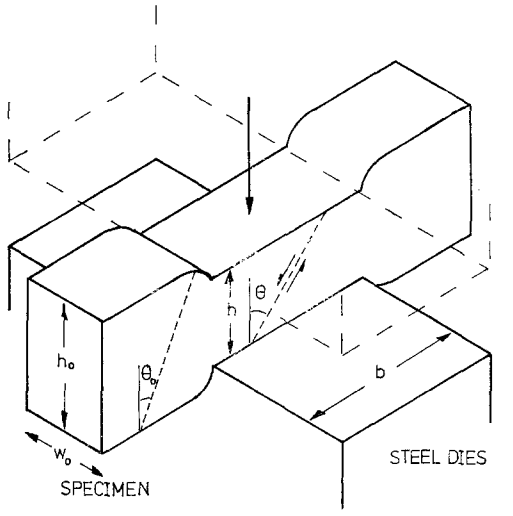

Figure 9 Schematic diagram of the dies used for the compression of specimens cut out of the oriented sheets. The direction of molecular alignment (y) is indicated by the dashed line. $b = 3.0$ mm, $w_0 \sim 2$ mm and $h_0 \sim 2$ mm.

not undergo plastic deformation as described below.

5.2. Compression-oriented sample

The three curves of stress against θ for this material are plotted as the middle set of curves in Fig. 10. The curve for a starting angle of about 20° does not show a load drop as in the case of the annealed material. The curves do not form a common envelope and they do not follow the theoretical curve which in this case is the middle dashed line fitted for a τ of 8.5 MNm^{-2}.

5.3. Draw-oriented material

The three curves for this material are plotted as the bottom set of curves in Fig. 10. Again they do not form a common envelope or coincide with the dashed line and there is no load drop for the 20° sample. The dashed curve is drawn for a critical resolved shear stress of 6 MNm^{-2}.

6. Simultaneous wide- and small-angle X-ray diffraction

Wide- and small-angle X-ray diffraction patterns of each of the three types of oriented material were taken before deformation and after deformation when the specimens had been allowed to relax, using Cu Kα radiation. All photographs were taken with the beam perpendicular to the chain direction (i.e. along x). The angle between the compression direction and the

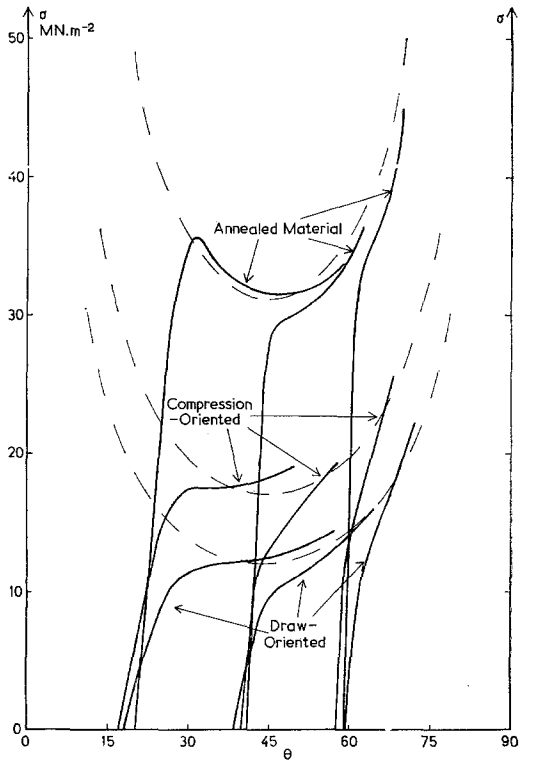

Figure 10 Plots of true stress against θ for each of the three types of oriented material using samples with values of θ_0 approximately equal to 20°, 40° and 60°. θ has been calculated from the change in h assuming Equation 14 to be valid. The dashed lines are the best fit of Equation 24 choosing appropriate values of τ for each of the three materials.

chain direction, θ, is measured using wide-angle diffraction and ϕ, the angle between the lamella normal and the compression direction, is measured from small-angle patterns.

6.1 Annealed material

The diffraction patterns for this material before deformation, taken with the beam along the x direction are shown in Fig. 8a. It can be seen that the small-angle pattern is quite well defined and is consistent with the model of the structure being made up of some lamellae perpendicular to the c-direction ($\theta_0 = \phi_0$). After deformation it can be seen that the direction of the lamella normals is no longer parallel to the chain direction. This implies that deformation by chain slip has taken place, since this is the only mechanism that causes ($\theta - \phi$) to change. From Table I it can be seen that measured values of θ

TABLE I The measured values of θ and ϕ were obtained from the photographs in Figs. 6, 7 and 8 and the calculated values were obtained by assuming that the permanent plastic strain is due only to chain slip, and using Equations 13, 14, and 15. The discrepancies in ϕ_1 imply that some fibrillar slip is occurring.

Specimen		h_0	h_1	θ_0	θ_1	ϕ_0	ϕ_1
Annealed	Meas.	1.317 mm	0.954 mm	17.5°	48.5°	19°	22.5°
	Calc.				46.5°		13°
Compression-oriented	Meas.	1.739 mm	1.476 mm	18.5°	38.5°	15°	23°
	Calc.				36°		12°
Draw-oriented	Meas.	1.995 mm	1.675 mm	20°	30.5°	17°	16°
	Calc.				38°		13°

and ϕ agree quite well with the values calculated using Equations 13, 14, and 15 for chain slip. This implies that chain slip is the major mechanism; the discrepancy in ϕ suggests that there may also be a small component of fibrillar slip.

6.2. Compression-oriented material

Fig. 7a shows a pair of X-ray diffraction patterns taken with the beam perpendicular to the chain direction and the compression direction. The small-angle pattern is not very well defined, indicating that the lamella structure perpendicular to the chain direction is not very well defined. From the patterns after deformation (Fig. 7b) it can be seen that the direction of the normals has again diverged from that of chain direction. From Table I it can be seen that the values of θ and ϕ which have been measured agree fairly well with the calculated values using the equations for chain slip. This again implies that this is the major deformation mechanism.

6.3. Draw-oriented material

The diffraction patterns for this material are given in Fig. 6 and it can be seen that the lamella structure is not very well defined. There is also an intense void streak perpendicular to the chain direction. After deformation the direction of the lamella normals is no longer parallel to the chain direction. Exact measurements are difficult but it does appear that there has been at least some chain slip. Measurements of the change in θ do not agree very well with the calculated values. The measured value of θ_1 is less than the calculated value and this implies that as well as some chain slip there has also been a certain amount of permanent lamella slip.

6.4. Discussion

The stress-strain results for the annealed sample presented in Section 5.1 are closely analogous to those that would be obtained from a perfect crystal undergoing single slip [5]. They imply that the value of τ being measured (15.5 MNm^{-2}) corresponds to the critical resolved shear stress for slip in the chain direction in polyethylene crystals as has already been suggested by two of us [4]. This conclusion is fully consistent with the X-ray results presented in Section 6.1.

For the other two materials the results in Sections 5.2 and 5.3 show that the stress-strain behaviour diverges widely from what would be expected from a single crystal, and the τ-values for flow are considerably lower. From the X-ray results it is evident that nevertheless some crystal slip in the chain direction is taking place. The reasons for the low flow stress are not clear. It could be because in these materials, which have not been annealed, the crystallites are very small and imperfect, the alignment between them is imperfect and the cohesion is poor.

7. Measurement of θ under load

A rig was constructed which enabled the angle between the chain direction and the compression direction to be measured by X-rays while the specimen was under load. The dies had the same dimensions as those described in Fig. 9 which meant that identical specimens could be used and it was hoped that results could be directly compared with the stress-strain work. The lower die was fixed but the upper was free to move and its position was registered by a dial gauge. The X-rays were sent through the centre of the specimen in a direction perpendicular to the face seen in Fig. 9. θ was measured from the angle which the $hk0$ reflections make with the compression direction. With unfiltered Cu radiation θ could be measured using exposures as short as 1 min.

7.1. Annealed material

The variation of θ with strain for a specimen with θ_0 equal to 16° is shown in Fig. 11. The specimen

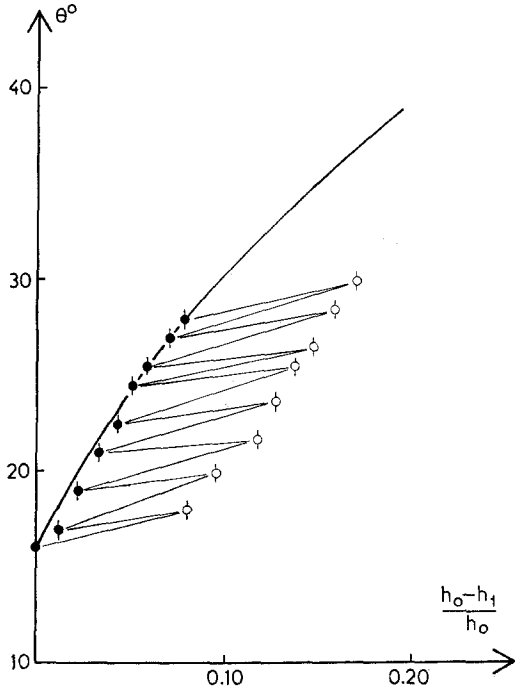

Figure 11 Variation of θ with nominal compressive strain for an annealed sample with $\theta_0 = 16°$. The open circles are measurements while specimen was under load. The solid circles are values measured when the specimen was allowed to relax. The thick line is the value of θ calculated by using Equation 14 with the measured values of h.

was loaded up to a strain of approximately 8% and held at this strain for 1 min while an X-ray photograph was taken. It was then unloaded and allowed to relax for 10 min after the end of which another diffraction photograph was taken. The specimen was then loaded up to a further 8% strain and the process repeated seven times. At the end of the experiment the specimen had a permanent plastic strain of about 8% but the bulging was less than 3%. A specimen which was strained in steps of about 8% but was not allowed to relax between each step was found to have bulged quite severely. It was taken to a permanent plastic strain of 28% and there was an increase in width of over 18%. This means that in this case the deformation was far from plane strain. During the experiment the specimen was held under load for over 1 h. It appears that the bulging may be a time-dependent process. In order to compare the results from this experiment with results obtained from the stress-strain work it is important that both experiments should have taken place on the same time-scale.

The thick line in Fig. 11 is calculated from Equation 14 assuming that the deformation has taken place by simple shear parallel to the chain direction. It can be seen that the points for θ relaxed lie quite close to the curve whereas the points obtained for θ under load fall a long way below the curve. This implies that the process which gives rise to the permanent plastic strain is either chain slip or fibrillar slip and since θ does not rotate when the material is under load by as much as is predicted by Equation 14, it implies that another process is taking place under load. Lamella slip causes θ to rotate in the opposite sense compared with the other two mechanisms. Lamella slip could therefore be taking place under load. It appears from the results in Fig. 11 that this process of lamella slip is reversible and the main process responsible for the elastic strains in the specimens. This may be contrasted with work on low-density polyethylene [2] in which both lamella slip and chain slip are found to be almost completely reversible.

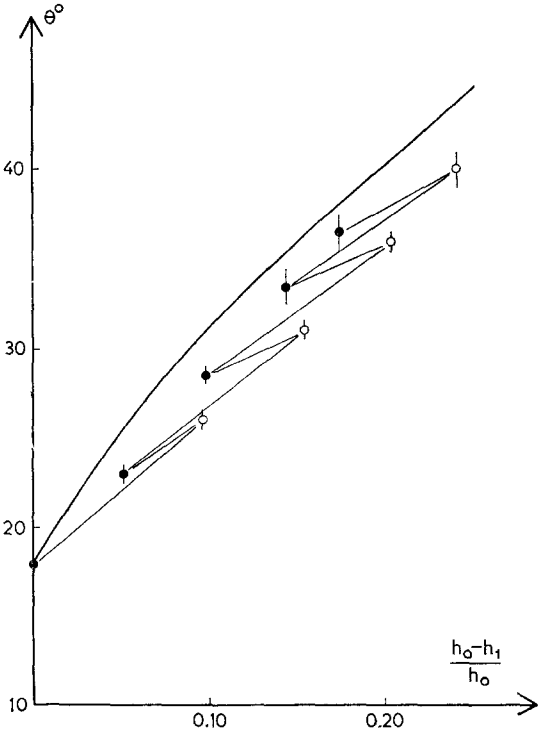

Figure 12 Variation of θ with compressive strain for a draw-oriented sample with θ_0 equal to 18°. The notation is the same as in Fig. 11.

7.2. Draw-oriented material

A similar experiment to that described in Section 7.1 was carried out on a specimen of draw-oriented material. The results for a specimen with a starting value of θ of 18° are shown in Fig. 12. The specimen was again loaded up to a strain of 8%, a photograph taken, and the specimen then allowed to relax. In this case the residual strain after relaxation was considerably greater. For the pressure-annealed material after eight steps there was a permanent plastic strain of 8% whereas for this material a residual strain of 17% was obtained after only five steps. At this strain the bulging was only about 1% which meant that the deformation was very close to plane strain. From Fig. 12 it can be seen that even the points which correspond to the material in a relaxed state fall some way below the line calculated for simple shear parallel to c. This implies that as well as there being some permanent chain or fibrillar slip there is also some permanent lamella slip.

8. Calculation of the magnitudes of the shear strains

The experiments in Section 7 were carried out by making small finite changes in h which cause small finite changes in θ. The analysis in Section 3 which can be used to calculate the values of the various shear strains, assumes that deformation has taken place in infinitesimally small steps and so in order to analyse the data from Section 7 several approximations must be made. It is necessary to use the mean values of h, θ and ϕ during each step instead of the values at the beginning of the step. θ and h are readily measured experimentally, but it is difficult to measure ϕ since it can only be found by taking low-angle X-ray diffraction photographs which require very long exposure times. If it is assumed that the amount of shear due to any one particular process is very small, the other two shears can be calculated by measuring any two of the three variables (normally h and θ). The low-angle X-ray results in Section 6 show that interfibrillar shear is not normally very large and so for the purposes of the calculations it has been assumed to be negligible ($\delta\gamma_F = 0$).

In order to calculate $\delta\gamma_L$ and $\delta\gamma_C$, Equations 22 and 23 are used with mean values of h and θ, and it has been assumed that initially $\phi = \theta$. It is not possible to measure ϕ but it can be calculated

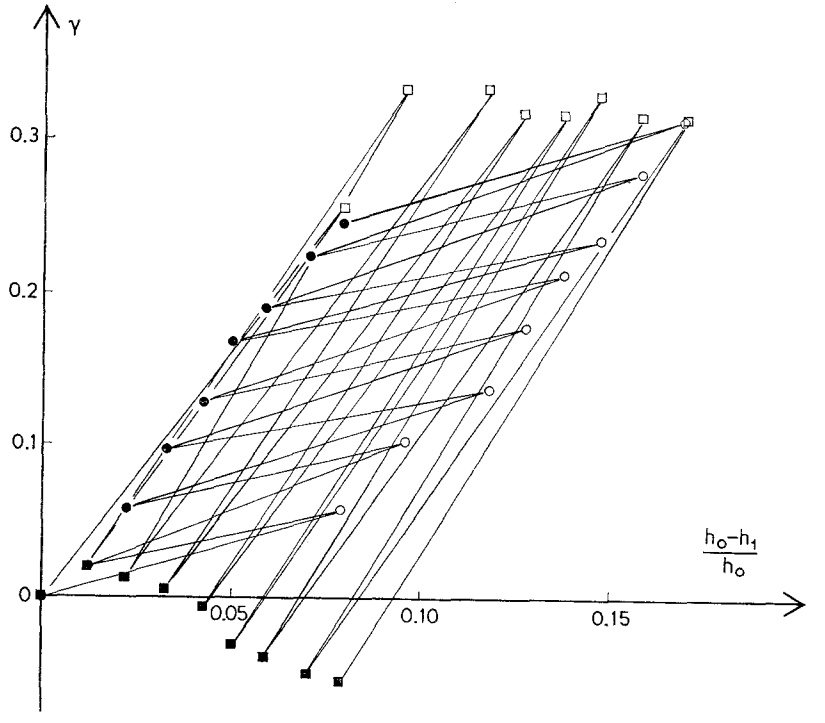

Figure 13 Calculated values of γ_L and γ_c as a function of strain for the annealed material using the data from Fig. 11.
○ – γ_c when the specimen is under load
● – γ_c when the specimen is relaxed
□ – γ_L when the specimen is under load
■ – γ_L when the specimen is relaxed.

from Equation 19 when $\delta\gamma_C$ and $\delta\gamma_L$ have been evaluated. An iterative process has been used to find the successive values of ϕ. By adding the calculated value of $\delta\phi$ to the original value of ϕ a value of ϕ for the end of a particular step is obtained. This is then used to calculate a mean value of ϕ which is used to calculate better values of $\delta\gamma_C$ and $\delta\gamma_L$. These new values of $\delta\gamma$ are used to find new values of ϕ. This process is repeated until the difference in successive values of ϕ is less than 10^{-6} of one degree.

The assumption that there has been no permanent fibrillar slip can be checked at the end of the experiment by measuring ϕ and comparing it with the final computed value. It is not possible to decide whether or not fibrillar slip takes place under load without measuring ϕ under load.

8.1. Results of the calculations for the annealed material

The calculated values of γ have been added for successive steps and plots of γ_C and γ_L against strain are given in Fig. 13 using the data from Fig. 11. It can be seen that under load γ_L is quite large (about 0.31) but when the material is allowed to relax γ_L decreases to a very small value and after four steps starts to go slightly negative. In contrast γ_C builds up gradually throughout the test but it decreases slightly on allowing the material to relax. This could be due to reversible chain slip or reversible fibrillar slip. It is not possible to decide which of these two processes takes place as this can only be done by measuring ϕ directly while the specimen is under load. The computed value of ϕ at the end of the experiment was 13.5° which agrees well with the

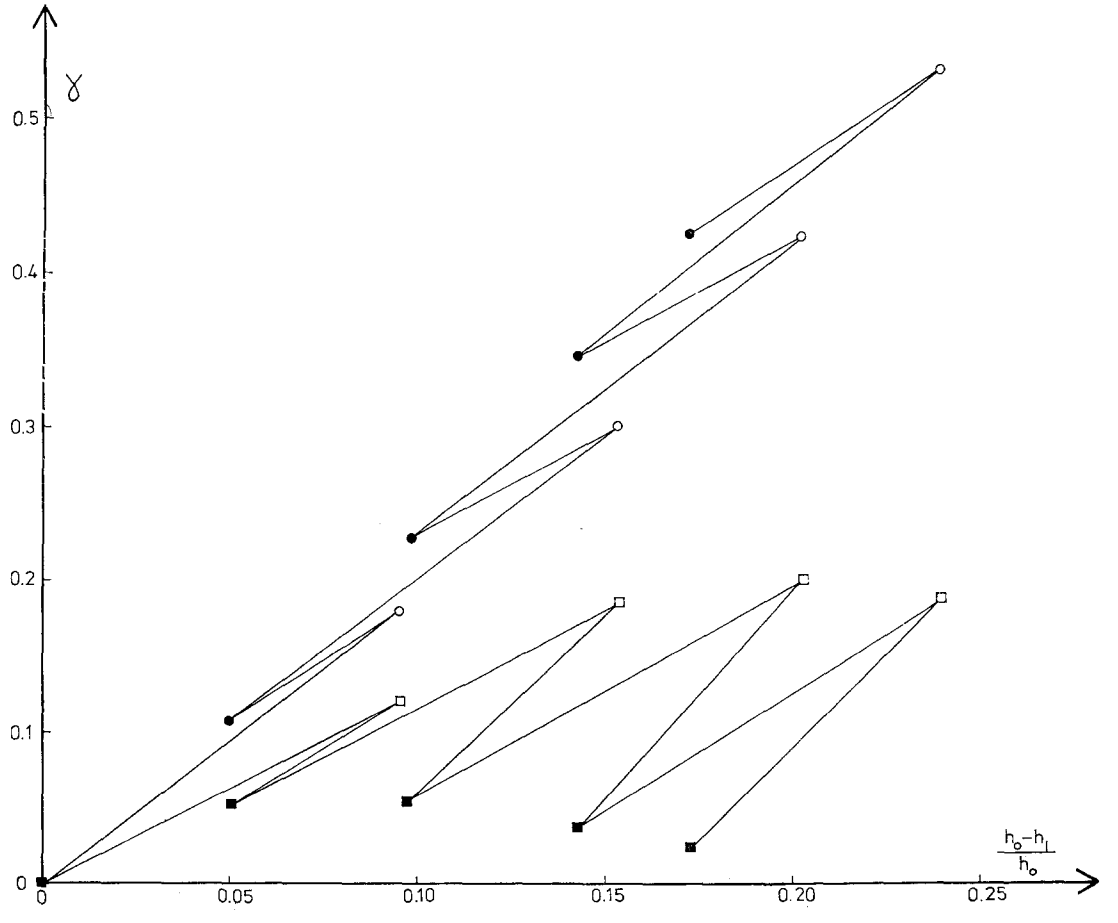

Figure 14 Calculated values of γ_C and γ_L as a function of nominal strain for the draw-oriented sample using the data from Fig. 12. The notation is identical to that used in Fig. 13.

measured value of $15 \pm 2°$ and implies that permanent fibrillar slip is only very small.

After deformation and when the material is in a relaxed state the permanent plastic strain appears to be almost entirely accounted for by chain slip whereas under load most of the elastic strain appears to be due to elastic lamella slip.

8.2. Results for the drawn material

Calculations from the data in Fig. 12 for the instantaneous values of γ_C and γ_L as a function of strain are plotted in Fig. 14. The behaviour of this material is similar to that of the annealed material. The value of γ_C increases steadily with strain and is only slightly reversible on unloading. For the draw-oriented material the increase of γ_C with strain is more rapid than in the annealed material. γ_L is less reversible than for the annealed material and there is some residual lamella shear strain when the material is relaxed. There is evidently permanent lamella slip in the specimen.

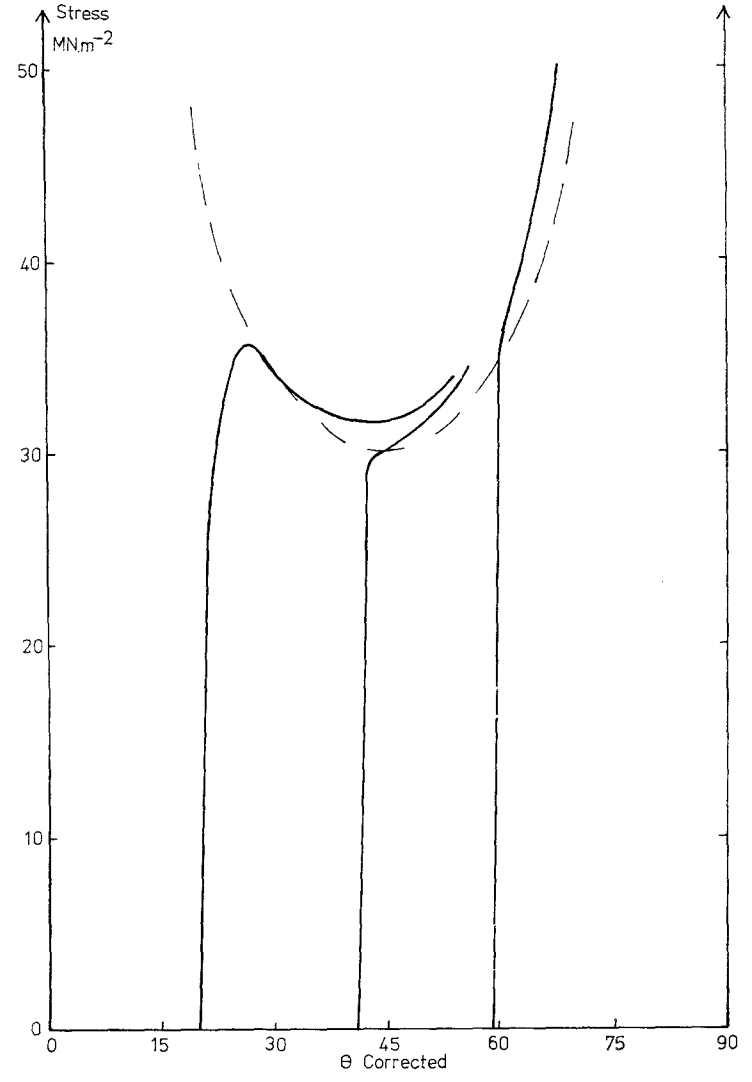

Figure 15 The corrected plot of stress against θ for the annealed material. θ-values have been corrected by subtracting 5 degrees from the values of θ used in Fig. 10 to account for the effect of elastic lamella slip. The dashed line is plotted using Equation 24 so that it passes through the yield points of each curve. This gives a value of τ equal to 15.0 MNm^{-2}.

8.3. Corrected curves of stress against θ for the annealed material

In Fig. 10 where values of the flow stress are plotted against θ the values of θ were obtained by assuming that the only deformation process operating under load was chain slip and using Equations 2 or 14 to calculate θ from the measured change in h. For the annealed sample it can be seen that the calculated increase in θ on loading to the yield point is very approximately 8°.

However, in Fig. 11 it can be seen that the actual change in θ occurring on loading to yield is less than 3° (the discrepancy is due to lamellar slip) so that the curves in Fig. 11 should be shifted to the left by approximately 5° if they are to be a plot of stress against the instantaneous value of θ under load. In Fig. 15 this 5° shift has been made and the data re-plotted.

The correction is not very rigorous since it assumes that the discrepancy will be the same for all values of θ but it does allow a better fit to be obtained with the theoretical Schmid and Boas curve. In this instance a value of 15.0 MNm^{-2} has been taken to make the theoretical curve pass as nearly as possible through the yield points of the plots of stress against θ.

After the yield point the curves rise above the theoretical line. This could mean that a certain amount of strain-hardening is taking place. Bowden and Young [4] have shown that there is a small strain-rate dependence of the critical resolved shear stress for [001] slip. When the height of the sample has been reduced by 50% the shear strain rate is doubled. This would cause an increase in the measured critical resolved shear stress at higher strains but it appears that even allowing for the strain-rate effect there is some strain-hardening in the material itself.

There is no clear evidence for any asymmetry in the envelope of the experimental curves in Fig. 15, which if it were present would imply that the yield stress increased with the normal pressure on the slip plane [6]. This asymmetry can be seen in the curves in Fig. 10 for the un-annealed materials.

9. Conclusions

The conclusions of the work presented here may be summarized as follows.

In oriented and annealed samples of high density polyethylene deformed by a stress system that favours shear parallel and perpendicular to the chain direction elastic deformation occurs primarily by shear of the lamella crystals over each other. This shear strain is fully recoverable on unloading. Such a result is consistent with the concept of a structure consisting of lamella crystals linked together by tie molecules which permit only a limited amount of shear. The principal mechanism of plastic deformation is by [001] crystallographic slip (in the chain direction) in the crystals themselves at a constant critical resolved shear stress (CRSS) of 15 MNm^{-2}. This shear deformation is not recoverable on unloading. Plastic deformation by this mechanism can continue to large strains (shear strains of the order of unity) with very little strain hardening.

In oriented samples of polythene that have not been annealed the structure is not so clearly defined and the deformation behaviour is more complicated. Some [001] chain slip takes place in the crystalline regions but the measured CRSS for flow is considerably lower (6 to 9 MNm^{-2}) possibly because the crystallites are very small and imperfect, possibly because the structure contains stress-concentrating voids or other regions of weakness. Chain slip in unannealed materials is partially reversible on unloading. Lamella slip also takes place under load but is only partially recovered on unloading.

Acknowledgements

The authors would like to thank Dr G. W. Groves for valuable discussion. The work was carried out with the help of support from the Ministry of Defence (Procurement Executive) and equipment grants from the SRC.

References

1. A. PETERLIN, *J. Mater. Sci.* **6** (1971) 490.
2. A. KELLER and D. P. POPE, *ibid* **6** (1971) 453.
3. I. L. HAY and A. KELLER, *ibid* **1** (1966) 41.
4. P. B. BOWDEN and R. J. YOUNG, *Nature, Physical Science* **229** (1971) 23.
5. E. SCHMID and W. BOAS, "Plasticity of Crystals" (Chapman and Hall, London, 1968).
6. T. HINTON and J. G. RIDER, *J. Appl. Phys.* **39** (1968) 4932.

Received 22 March and accepted 22 June 1972.